Theoretical studies of the physical properties of solar material $CuAlS_2$

G. Yan [a], S. R. Zhang [a,*], H. J. Hou [b], Z. F. Yin [b], H. L. Guo [c]
[a] *School of Physics, Electronics and Intelligent Manufacturing, Huaihua University, Huaihua, 418008, China*
[b] *School of Materials Engineering, Yancheng Institute of Technology, Yancheng, 224051, China*
[c] *College of Electronic and Information Engineering, Yangtze Normal University, Fuling, 408000, Chongqing, China*

The theoretical approach was employed to comprehensively investigate the structural, dynamical, band structure, optical characteristics, and elastic anisotropy of $CuAlS_2$. The determined lattice parameters (*a* and *c*), elastic properties exhibit with the available data. The band structure and density of state indicates that $CuAlS_2$ exhibits semiconductor properties, characterized by a direct band gap measuring approximately 1.791 eV. The mechanical stability and optical properties of $CuAlS_2$ was calculated and analyzed.

(Received October 29, 2024; Accepted January 8, 2025)

Keywords: $CuAlS_2$, Electronic structure, Optical, Anisotropy

1. Introduction

Scientists have shown significant interest in the versatile technological applications of chalcopyrite semiconductors, which are characterized by the formula $A^{XI}B^{XII}C^{VI2}$. Ternary chalcopyrites are widely recognized for their capacity to be utilized in light-emitting diodes (LEDs), solar panels, and devices with nonlinear optical properties [1-4]. $CuAlS_2$ is classified as a member of the chalcopyrite family. Numerous investigations have undergone examination [5, 6] to explore the electronic, electrical, and optical characteristics of $CuAlS_2$ under normal atmospheric conditions. S. Sugan and colleagues conducted a study on the optical characteristics of $CuAlS_2$ at ambient temperature by employing the experimental technique [7]. Jaffe et al employed the theoretical technique to explore chemical properties of $CuAlS_2$[8]. Abdellaoui et al. investigated the $CuAlX_2$ (X = S, Se, Te) using the theoretical approach to analyze their structural, and physical properties [9]. Recently, Geng et al have conducted a analysis on the properties of tetragonal $CuAlS_2$ under various pressures [10]. There has been a lack of extensive research on the anisotropy and dynamic properties of $CuAlS_2$. In this study, we examined the anisotropy of $CuAlS_2$ in terms of its structure and elasticity through first-principles calculations. DFT has demonstrated its efficacy in investigating the characteristics and mechanical behavior of various materials, including theoretical examinations on comparable substances [11].

* Corresponding author: zefer1979@163.com
https://doi.org/10.15251/CL.2025.221.33

2. Computational methods

In this study, the theoretical method is employed within the DFT framework to investigate the characteristics of $CuAlS_2$. The analysis is conducted using the CASTEP code developed by Cambridge for calculating total energy [12-13]. The Perdew-Burke-Ernzerhof (PBE) functional is employed in the generalized gradient approximation (GGA) to describe the exchange-correlation energy [14]. We utilize Vanderbilt-type ultrasoft pseudopotentials for characterizing the interactions between electrons and ions [15]. In the computation, the threshold was established at 500.00 eV and the Monkhorst-Pack mesh with *k* 7×7×6 [16]. In this study, we performed dynamical properties calculations using the VASP code [17] and phonopy code [18], employing DFPT within the linear response framework. During the dynamical calculations, we have pre-expanded the 2×2×1 super cell of 64 atoms to enhance result accuracy.

3. Results and discussion

3.1. Structural model

In Table 1, we presented the findings alongside the experimental data [8] that is accessible and other theoretical outcomes [9-10, 19]. The calculated lattice parameters (*a*, *c*) show a maximum relative difference of 2% compared to their corresponding experimental counterparts[8]. All the findings indicate that the results derived from GGA calculation exhibit a higher level of concordance with the available data.

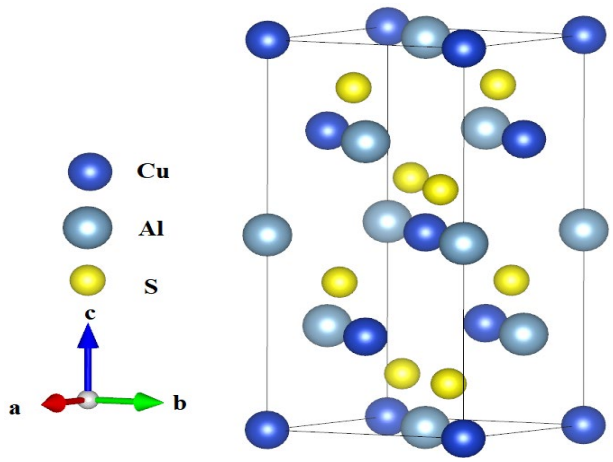

Fig. 1. The structural model of $CuAlS_2$

Table 1. The lattice parameters a and c (in Å) were determined, along with the ratio of c/a, for $CuAlS_2$.

	a (Å)	*c* (Å)	*c*/*a*
Present	5.3335	10.5489	1.9778
Theo.[9]	5.18	10.35	1.9981
Theo.[10]	5.414	10.507	1.9407
Theo.[19]	5.341	10.57	1.9790
Exp.[8]	5.31	10.42	1.9623

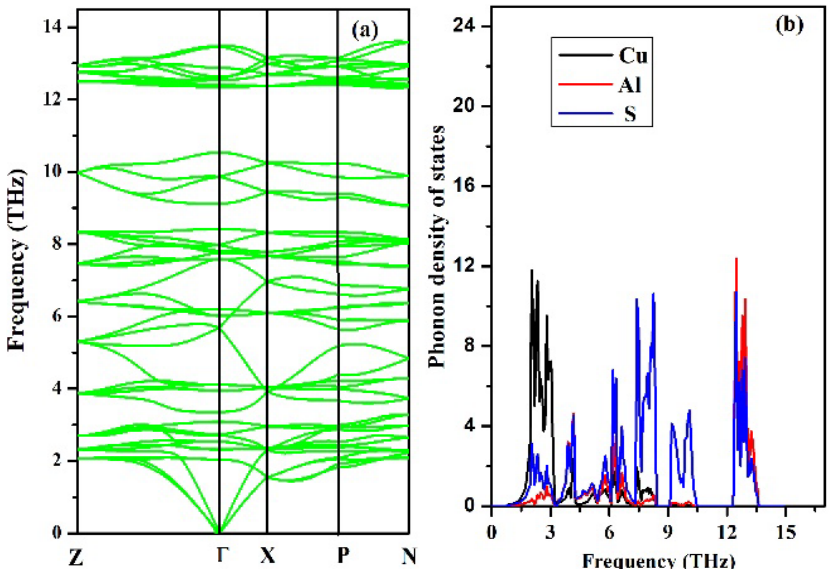

Fig. 2. Phonon dispersion curve and Phonon density of states of $CuAlS_2$.

Fig. 2 showcases dynamical properties calculations for $CuAlS_2$ in its state of equilibrium. It can be observed that the material $CuAlS_2$ demonstrates dynamic stability, as there is an absence of detected imaginary phonon frequencies within it. The $CuAlS_2$ material exhibits frequency gaps in its phonon dispersion curves and is characterized by three distinct groups of bands in its partial phonon density of states. The dominant factors influencing the high frequency modes (12-13 THz) are attributed to atoms Al and S. The identification of the range of modes within the medium frequency group, spanning from 3 to 10 THz, is influenced by the combined contributions of Al and S atoms. The Cu and Al atoms combine the low frequencies ranging from 0-3 THz.

3.2. Electronic properties

In Fig. 3, $CuAlS_2$ displays properties typical of a direct bandgap semiconductor. The value obtained for the bandgap *E*g is 1.791 eV, despite employing the generalized gradient approximation (GGA), it slightly deviates from the experimental measurement of 3.49 eV[8].

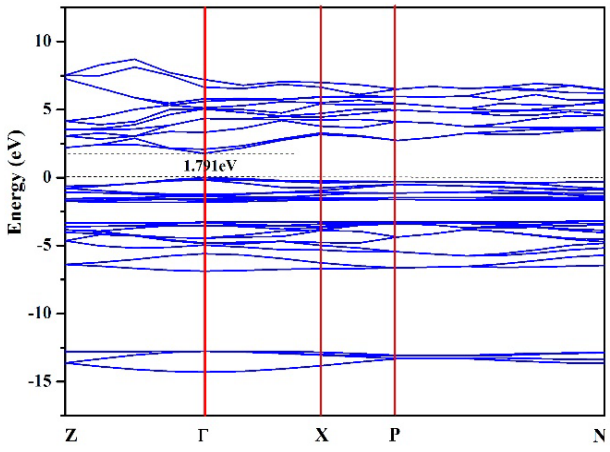

Fig. 3. Band structure of $CuAlS_2$.

In Fig. 4, the dominant composition of higher valence band in $CuAlS_2$ is attributed to the presence of Cu 3d and S 3p orbitals. Other components include Cu 3p, Al 3p, and Al 3s orbitals. The major portion of the lower valence band is composed of S 3p, Cu 3d, Al 3s, and Al 3p orbitals. Furthermore, Cu 4s and Cu 3p orbitals also make slight contributions. In addition, the valence band of $CuAlS_2$ is primarily composed of S 3s, Al 3p, and Al 3s in the energy range from -14.5eV to -12.8eV. This particular valence band is located far away from other valence bands and exhibits minimal interaction with them. In contrast, Fig. 4 illustrates that the conduction band of $CuAlS_2$ displays a relatively dispersed nature and consists mainly of Al 3p, Al 3s, Cu 3p, Cu 4s along with a small proportion of S 3p.

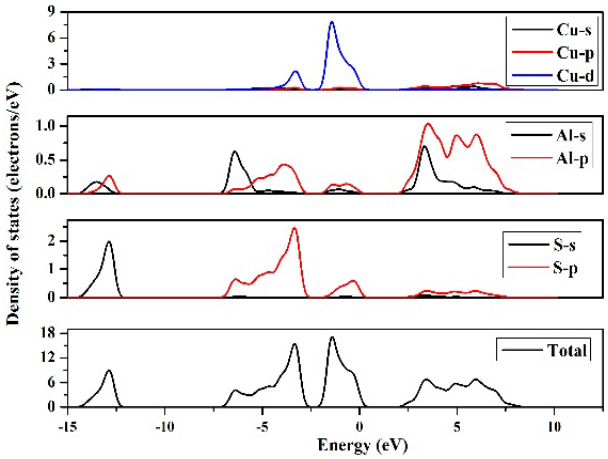

Fig. 4. Density of states of $CuAlS_2$.

3.3. Optical properties

The following is the dielectric function expressed by complex expression [20]

$$\varepsilon(\omega) = \varepsilon_1(\omega) + i\varepsilon_2(\omega) \tag{1}$$

It can be used to represent the ability of $CuAlS_2$ to store electromagnetic fields, and it is what we call the dielectric constant. It represents the loss caused by the lagging response caused by the crystal polarizability not keeping up with the external field changes.

Both the real $\varepsilon_1(\omega)$ and imaginary $\varepsilon_2(\omega)$ of dielectric function is depicted in Fig.5. As depicted in the diagram, the value of $\varepsilon_1(0)$, which represents the static dielectric constant, is measured to be 6.39. Before the photon energy surpasses 3.18 eV, there is a progressive rise in the real part ε_1 as the photon energy increases until it reaches its peak value of 9.44 at 3.07 eV. After that, the real part ε_1 gradually decreases, rising and then decreasing at about 5 eV of photon energy, until it reaches the lowest point of -3.093 at 9.72 eV of photon energy. On the other hand, the imaginary part rises first and then falls, reaching a maximum peak value of 10.83 when the photon energy is 6.71 eV.

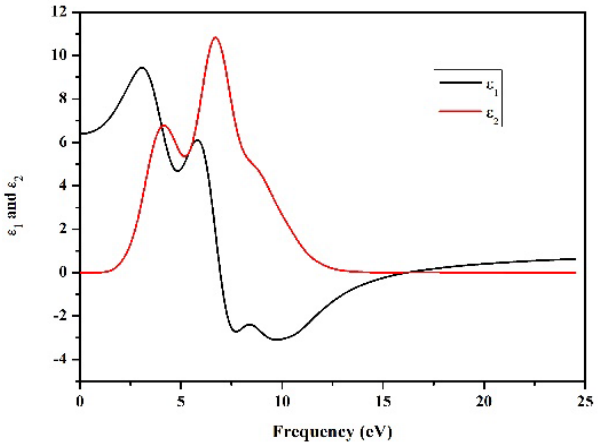

Fig. 5. The real part $\varepsilon_1(\omega)$ and imaginary part $\varepsilon_2(\omega)$ of the dielectric function of $CuAlS_2$.

The refractive index $n(\omega)$ and the extinction coefficient $k(\omega)$ are displayed in Fig. 6. When the photon energy is 3.22 eV, the maximum refractive index *n* is 3.12. Previously, there was a gradual rise in the refractive index as photon energy increased. *n* fluctuates greatly in the range of 3.34eV ~ 6.84eV, with a minimum value at first and then rising to the second peak value of 2.45; After this, the refractive index *n* decreases continuously until it drops to 0 when the energy is about 15 eV, and then gradually increases.

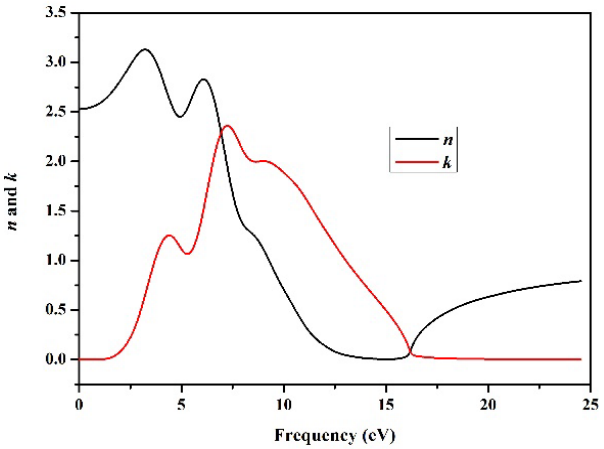

Fig. 6. The refractive index $n(\omega)$ and the extinction coefficient $k(\omega)$ of $CuAlS_2$.

The reflection coefficient *R* can be formulated based on *n* and *k*.

$$R = \frac{(n-1)^2 + k^2}{(n+1)^2 + k^2} \tag{2}$$

The absorption coefficient α represents the percentage of light absorbed when it is displaced in the crystal, and its mathematical expression is as follows:

$$\alpha = \frac{4k\pi}{\lambda_0} = \frac{\omega}{ne}\varepsilon_2(\omega) \tag{3}$$

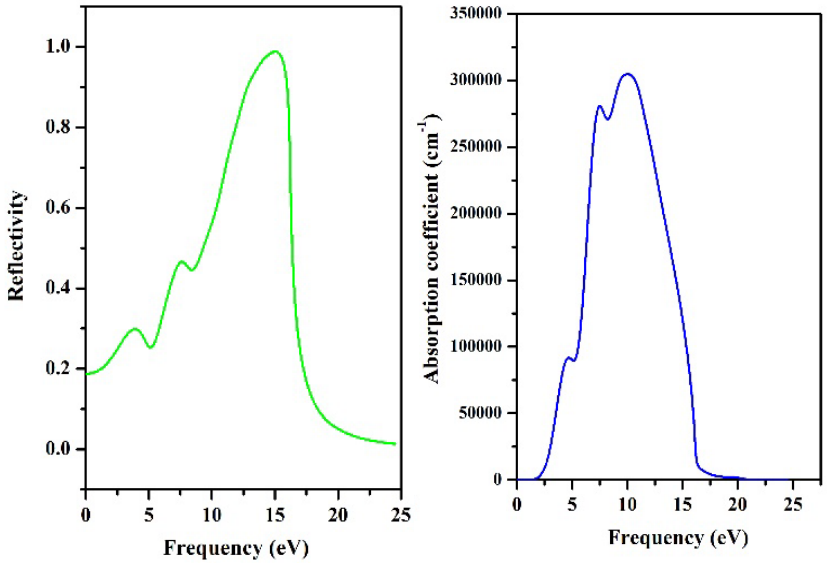

Fig. 7. Reflectivity spectrum $R(\omega)$ and absorption spectrum $\alpha(\omega)$ of $CuAlS_2$.

Fig. 7 illustrates the reflectivity and absorption spectra of $CuAlS_2$. We can find that the reflectivity spectrum has three peaks, corresponding to the highest peaks of n and k and the 15 eV where they decay rapidly together. When the reflectance reaches the highest peak, the refractive index and absorbance of the crystal are very low, because most of the light is reflected out. It is evident from the figure provided that for photon energies < 1.791 eV, α exhibits a value of zero. In this range, $CuAlS_2$ is transmitting. After 1.791 eV, α increases continuously with the increase of photon energy, until the photon energy reaches 4.63 eV, reaching the first peak of 91571.3 cm^{-1}, and then rising again after a short period of reduction, reaching the maximum absorption rate of 305443.4 cm^{-1} at 10.09 eV. The value of α exhibits a significant decline as the photon energy rises, eventually approaching zero.

3.4. Elastic properties

To the best of our understanding, chalcopyrite compounds exhibit six distinct components. These components are denoted as C_{11}, C_{33}, C_{44}, C_{66}, C_{12} and C_{13}. The elastic compliance tensor components of $CuAlS_2$ can be found in Table 2. The satisfaction of Born stability criteria [21] is necessary for the elastic stiffness tensor components in the tetragonal chalcopyrite lattice. The values obtained in Table 2 satisfy all the aforementioned limitations, suggesting that $CuAlS_2$ exhibits mechanical stability. The elastic constants derived from our computations and those obtained through other theoretical findings [9, 10, 22, 23] can be found in Table 2. By comparing, we found that the calculated results match the reference values very well, indicating the accuracy of our calculations.

Table 2. The elastic constants C_{ij} (GPa), linear compressibilities χ_a, χ_c (TPa^{-1}) and volume compressibilities , χ (TPa^{-1}) of $CuAlS_2$.

	C_{11}	C_{12}	C_{13}	C_{33}	C_{44}	C_{66}	χ_a	χ_c	χ
Present	108.44	61.39	64.79	108.81	53.21	38.8	0.0044	0.0040	0.0127
Theo.[22]	91.7	57.3	67	105.8	51.43	35.3	0.0057	0.0022	0.0137
Theo.[9]	133.001	80.762	84.552	135.064	56.543	53.762	0.0035	0.0031	0.0099
Theo.[10]	124.12	78.37	80.97	127.18	51.68	52.18	0.0037	0.0032	0.0105
Theo.[23]	108.2	57.3	60.8	117.9	55.1	54.7	0.0047	0.0036	0.0130

Table 2 displays the linear compressibilities χ_a and χ_c, which are observed along the *a* and *c* axes, as well as the volume compressibility χ [24]. The findings derived from this study appear to exhibit a significantly greater proximity to alternative theoretical values [9, 10, 22, 23]. This validates the current computations.

In addition, the bulk modulus *B* and shear modulus *G* of polycrystalline $CuAlS_2$ can be acquired through the Voigt, Reuss and Hill's study [25-27], resulting in values of 78.62 GPa and 37.56 GPa, respectively. The above values can be utilized for the analysis of the Poisson ratio *v* and Young's modulus *E*.

$$\nu = (3B - 2G) / (6B + 2G) \tag{4}$$

$$E = 9BG / (3B + G) \tag{5}$$

Table 3. Calculated bulk modulus B (GPa), Shear modulus G (GPa), Young's Modulus E (GPa), Poisson's ratio v, B/G ratio $CuAlS_2$.

	B_V	B_R	B	G_V	G_R	G	E	v	B/G
Present	78.63	78.6	78.62	40.55	34.17	37.56	97.20	0.3156	2.0931
Ref.[9]			100.03			40.443	106.919	0.321	2.4733

Table 3 presents the computed *B*, *G*, *E*, *v*, and *B*/*G* for $CuAlS_2$. It can be deduced that our findings are consistent with the previously reported results [9]. If $B/G < 1.75$, the material exhibits brittleness. When $B/G > 1.75$ [28], it indicates a ductile nature of the material. According to the information provided in Table 3, it can be inferred that $CuAlS_2$ exhibits ductility.

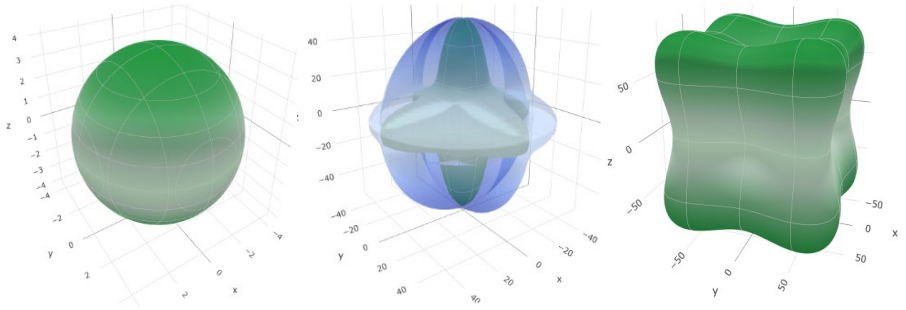

Fig. 8. The surface contours of β (TPa^{-1})(a), G (GPa) (b) and E (GPa) (c) of $CuAlS_2$. (linear compressibility).

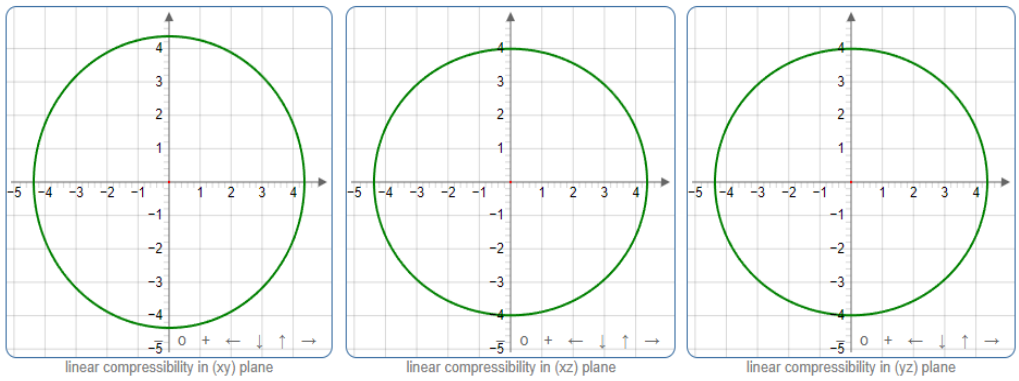

(shear modulus)

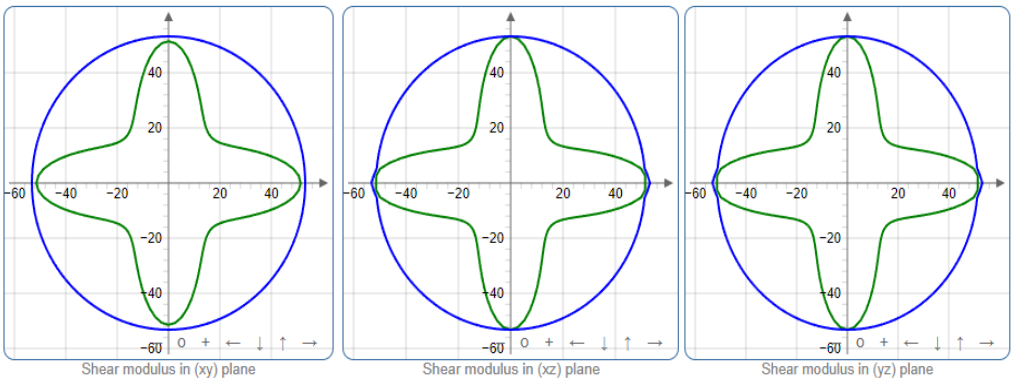

(Young modulus)

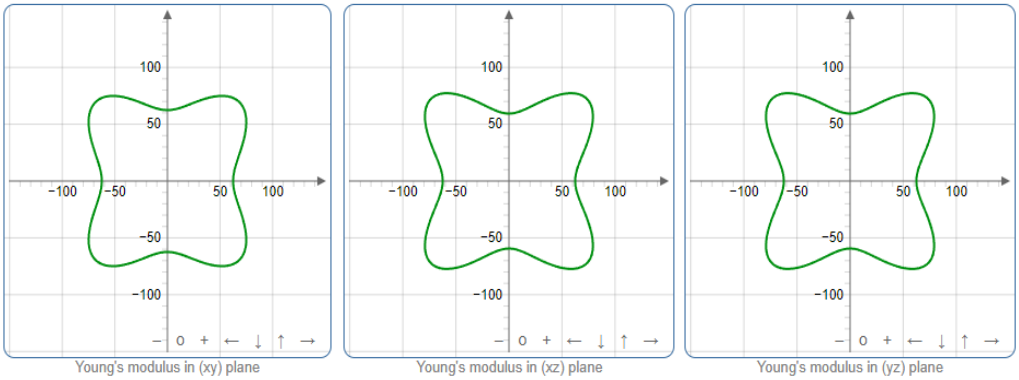

Fig. 9. Estimations of β (a) (TPa^{-1}), G (b) (GPa) and E (c) (GPa) in different planes.

The utilization of surface contours and Projections graphical depictions can effectively illustrate the elastic anisotropy displayed by crystals, specifically in terms of linear compressibility (β), E, and G. The ELATE software [29] is employed to input the matrix and facilitate the visualization of anisotropy with respect to β, G, E of $CuAlS_2$. The isotropic nature of crystals can be inferred from their graphical depictions in different plane and surface contours. The level of anisotropy rises with increasing deviation from these forms. Fig. 8-9 illustrates the directional dependence of β, G, E for $CuAlS_2$ in both Projections (xy-, xz-, and yz-planes) and 3D perspectives. Simultaneously, the linear compression anisotropy of $CuAlS_2$ was thoroughly evaluated through the analysis of β_{max}/β_{min}, G_{max}/G_{min} and E_{max}/E_{min}. A higher value of β_{max}/β_{min} indicates greater anisotropy in linear compression, which is also reflected in the corresponding values of G_{max}/G_{min} and E_{max}/E_{min}. The β_{max}/β_{min} is 1.0937, the G_{max}/G_{min} is 2.432; and the E_{max}/E_{min} values is 2.174, respectively. Based on the graphical plots in both Projections and 3D, it can be observed that $CuAlS_2$ exhibits anisotropy with the following order of $\beta < E < G$.

4. Conclusions

We have employed theory to conduct computations on the properties of $CuAlS_2$, including its structural characteristics, elasticity, band structure and optical behavior. The determined lattice parameters and elastic properties demonstrate concurrence with previously established theoretical values. The analysis of the electronic characteristics indicates that $CuAlS_2$ possesses band gap with a magnitude of 1.791 eV. The transmission of $CuAlS_2$ is observed for frequencies below 1.791 eV, as indicated by its optical properties. According to the given data on elastic constants, it can be deduced that $CuAlS_2$ demonstrates mechanical stability that closely aligns with its theoretical values

References

[1] N. Yamamoto, Proceeding of the Fourth International Conference on Ternary and Multinary Compounds, Ref. 11, Tokyo, 1980, p. 45.

[2] S. Wagner, J.L. Shay, P. Migliorato, H.M. Kasper, Appl. Phys. Lett. 25, 434 (1974); https://doi.org/10.1063/1.1655537

[3] B.R. Pamplin, T. Kiyosawa, K. Masumoto, Prog. Cryst. Growth Charact. 1, 331(1979); https://doi.org/10.1016/0146-3535(79)90002-9

[4] F. Abou-Elfotouh, D. J. Dunlavy, L. L. Kazmerski, D. Albin, K. J. Bachman, R. Menner J. Vac. Sci. Technol. A6, 1515(1988); https://doi.org/10.1116/1.575352

[5] S. Chichibu, M. Shishikura, J. Ino, S. Matsumoto, J. Appl. Phys. 70 1648 (1991); https://doi.org/10.1063/1.349531

[6] A. M. Andriesh, H. N. Syrbu, S. M. Iovu, E. V. Tazlavan, Crystals Phys. Stat. Sol. B 187, 83(1995); https://doi.org/10.1002/pssb.2221870107

[7] K. Sugan, K. Baskar, R. Dhanasekaran, J. Alloy Compd. 4, 129 (2015)

[8] J.E. Jaffe, A. Zunger, Phys. Rev. B 28, 5822(1983).

[9] A. Abdellaoui, M. Ghaffour, M. Bouslama, S. Benalia, A. Ouerdane, B. Abidri, Y. Monteil, J.

Alloys Compd. 487, 206(2009); https://doi.org/10.1016/j.jallcom.2009.08.141

[10] J. Geng, J. Wu, Chalcogenide Lett. 20 215 (2023); https://doi.org/10.15251/CL.2023.203.215

[11] H.J. Hou, W.X. Chen, M.H. Zhu, H.Y. Wang, X.W. Lu, S.R. Zhang, Vacuum 206, 111505 (2022)

[12] P. Hohenberg, W. Kohn Phys. Rev. B 136, 864 (1964); https://doi.org/10.1103/PhysRev.136.B864

[13] W. Kohn, L. J. Sham, Phys. Rev. A 140, 1133 (1965); https://doi.org/10.1103/PhysRev.140.A1133

[14] J. P. Perdew, K. Burke, M. Ernzerhof, Phys. Rev. Lett. 77, 3865 (1996); https://doi.org/10.1103/PhysRevLett.77.3865

[15] D. Vanderbilt, Phys. Rev. B 41, 7892 (1990); https://doi.org/10.1103/PhysRevB.41.7892

[16] M. C. Payne, M. P. Teter, D. C. Allen, T. A. Arias, J. D. Joannopoulos, Rev. Mod. Phys. 64, 1045 (1992); https://doi.org/10.1103/RevModPhys.64.1045

[17] G. Kresse, J. Furthmuller, Phys. Rev. B 54, 11169 (1996); https://doi.org/10.1103/PhysRevB.54.11169

[18] A.Togo, Phonopy. http://sourceforge.net/projects/phonopy/.

[19] A.S. Verma, Sheetal Sharma, R. Bhandari, B. K. Sarkar, V.K. Jindal, Mater. Chem. Phys. 132, 416 (2012); https://doi.org/10.1016/j.matchemphys.2011.11.047

[20] S.R. Zhang, D.P. Zeng, H.J. Hou, Y. Yu, Indian J. Phys. 94, 1335(2020); https://doi.org/10.1007/s12648-019-01575-8

[21] M. Born, K. Huang 1954 Dynamical Theory of Crystal Lattices (Oxford: Clarendon)

[22] A.S. Vermaa, Sheetal Sharma, R. Bhandari, B.K. Sarkar, V.K. Jindal, Mater. Chem. Phys. 132, 416 (2012); https://doi.org/10.1016/j.matchemphys.2011.11.047

[23] M. G. Brik, Phys. Status Solidi C 8, 2582 (2011); https://doi.org/10.1002/pssc.201084061

[24] H. Neumann, Cryst. Res. Technol. 39, 939 (2004); https://doi.org/10.1002/crat.200410280

[25] W. Voigt, Handbook of Crystal Physics, Taubner, Leipzig, 1928.

[26] A. Reuss, Z. Angew. Math. Mech 9, 49(1929); https://doi.org/10.1002/zamm.19290090104

[27] R. Hill, Proceedings of the Physical Society. Section A, 65, 349(1952); https://doi.org/10.1088/0370-1298/65/5/307

[28] S. F. Pugh, Philos. Mag. 45, 823 (1954); https://doi.org/10.1080/14786440808520496

[29] R. Gaillac, P. Pullumbi, F. X.Coudert, J. Phys.Condens. Matt. 28, 275201(2016); https://doi.org/10.1088/0953-8984/28/27/275201